Springer Proceedings in Physics 61

Springer Proceedings in Physics

Managing Editor: H. K. V. Lotsch

44 *Optical Fiber Sensors*
Editors: H. J. Arditty, J. P. Dakin, and R. Th. Kersten

45 *Computer Simulation Studies in Condensed Matter Physics II: New Directions*
Editors: D. P. Landau, K. K. Mon, and H.-B. Schüttler

46 *Cellular Automata and Modeling of Complex Physical Systems*
Editors: P. Manneville, N. Boccara, G. Y. Vichniac, and R. Bidaux

47 *Number Theory and Physics*
Editors: J.-M. Luck, P. Moussa, and M. Waldschmidt

48 *Many-Atom Interactions in Solids*
Editors: R .M. Nieminen, M. J. Puska, and M. J. Manninen

49 *Ultrafast Phenomena in Spectroscopy*
Editors: E. Klose and B. Wilhelmi

50 *Magnetic Properties of Low-Dimensional Systems II: New Developments*
Editors: L. M. Falicov, F. Mejía-Lira, and J. L. Morán-López

51 *The Physics and Chemistry of Organic Superconductors*
Editors: G. Saito and S. Kagoshima

52 *Dynamics and Patterns in Complex Fluids: New Aspects of the Physics-Chemistry Interface*
Editors: A. Onuki and K. Kawasaki

53 *Computer Simulation Studies in Condensed Matter Physics III*
Editors: D. P. Landau, K. K. Mon, and H.-B. Schüttler

54 *Polycrystalline Semiconductors II*
Editors: J. H. Werner and H. P. Strunk

55 *Nonlinear Dynamics and Quantum Phenomena in Optical Systems*
Editors: R. Vilaseca and R. Corbalán

56 *Amorphous and Crystalline Silicon Carbide III and Other Group IV – IV Materials*
Editors: G. L. Harris, M. G. Spencer, and C. Y.-W. Yang

57 *Evolutionary Trends in the Physical Sciences*
Editors: M. Suzuki and R. Kubo

58 *New Trends in Nuclear Collective Dynamics*
Editors: Y. Abe, H. Horiuchi, and K. Matsuyanagi

59 *Exotic Atoms in Condensed Matter*
Editors: G. Benedek and H. Schneuwly

60 *The Physics and Chemistry of Oxide Superconductors*
Editors: Y. Iye and H. Yasuoka

61 *Surface X-Ray and Neutron Scattering*
Editors: H. Zabel and I. K. Robinson

62 *Surface Science: Lectures on Basic Concepts and Applications*
Editors: F. A. Ponce and M. Cardona

63 *Coherent Raman Spectroscopy: Recent Advances*
Editors: G. Marowsky and V. V. Smirnov

64 *Superconducting Devices and Their Applications*
Editors: H. Koch and H. Lübbig

Volumes 1–43 are listed on the back inside cover

H. Zabel I. K. Robinson (Eds.)

Surface X-Ray and Neutron Scattering

Proceedings of the 2nd International Conference,
Physik Zentrum, Bad Honnef, Fed. Rep. of Germany,
June 25–28, 1991

With 120 Figures

Springer-Verlag
Berlin Heidelberg New York
London Paris Tokyo
Hong Kong Barcelona
Budapest

Contents

Conference Summary
By S.K. Sinha 1

Part I Surface Crystallography and Phase Transitions

Surface X-Ray Crystallography and STM Images
By R. Feidenhans'l (With 3 Figures) 5

Determination of Metal Adsorbed Surfaces by X-Ray Diffraction
By T. Takahashi (With 5 Figures) 11

Au Adsorption on Si(111) Studied
by Grazing Incidence X-Ray Diffraction
By C. Schamper, D. Dornisch, W. Moritz, H. Schulz, R. Feidenhans'l,
M. Nielsen, F. Grey, and R.L. Johnson (With 3 Figures) 17

Grazing Incidence X-Ray Scattering Study of Staircases
of Steps on Si(001) Surfaces
By G. Renaud, P.H. Fuoss, J. Bevk, and B.S. Freer
(With 2 Figures) 21

Structure and Phase Transitions of Ge(111) and Si(111) Surfaces
at High Temperatures
By K.I. Blum, D.Y. Noh, A. Mak, K.W. Evans-Lutterodt, J.D. Brock,
G.A. Held, and R.J. Birgeneau (With 3 Figures) 27

Anomalous Scattering Applied to Co/Si(111) Interface Structure
By N. Jedrecy, A. Waldhauer, M. Sauvage-Simkin, R. Pinchaux,
and V.H. Etgens (With 2 Figures) 33

X-Ray Reflectivity Studies of Au Surfaces
By D.L. Abernathy, D. Gibbs, G. Grübel, K.G. Huang, S.G.J. Mochrie,
B.M. Ocko, A.R. Sandy, and D.M. Zehner (With 5 Figures) 37

Crystal Truncation Rod as a Convolution
of Three-Dimensional Bravais Lattice with X-Ray Reflectivity
By Hoydoo You 47

Extended X-Ray Reflectivity Analysis of Si(111)7×7
By I.K. Robinson and E. Vlieg (With 3 Figures) 51

Critical Phenomena at Surfaces and Interfaces
By R. Lipowsky 57

Surface-Induced Order Observed on a $Cu_3Au(001)$ Surface
By K.S. Liang, H.H. Hung, S.L. Chang, Z. Fu, S.C. Moss,
and K. Oshima (With 2 Figures) 65

Thermal Dynamics of (110) fcc Metal Surfaces
By K. Kern 69

Facet Coexistence in the Roughening Transition of Ag(110)
By H.G. Hörnis, E.H. Conrad, E. Vlieg, and I.K. Robinson
(With 5 Figures) 73

Kinetics of Ordering with Random Impurities: Pb on Ni(001)
By P.W. Stephens, P.J. Eng, and T. Tse (With 3 Figures) 79

Part II **Reflectivity**

Anomalous Reflectivity:
A New Method for Determining Density Profiles of Thin Films
By S.K. Sinha, M.K. Sanyal, K.G. Huang, A. Gibaud, M. Rafailovich,
J. Sokolov, X. Zhao, and W. Zhao (With 3 Figures) 85

Specular and Diffuse Scattering Studies of Multilayer Interfaces
By M.K. Sanyal, S.K. Sinha, A. Gibaud, S.K. Satija, C.F. Majkrzak,
and H. Homa (With 3 Figures) 91

Scattering Cross-Section of X-Rays and Neutrons
for Grazing Incidence onto Thin Films
By A. Haase and S. Dietrich 95

Total Neutron Reflection: Experiments and Analysis
By G.P. Felcher, W.D. Dozier, Y.Y. Huang, and X.L. Zhou
(With 3 Figures) 99

Profile Refinement in Neutron Reflectivity
and Grazing Angle Diffraction
By J.F. Ankner (With 1 Figure) 105

Part III **Surface X-Ray Standing Waves**

X-Ray Standing Wave Studies of the Liquid/Solid Interface
and Ultrathin Organic Films
By M.J. Bedzyk (With 3 Figures) 113

Glancing-Incidence X-Ray Analysis of Layered Materials
By D.K.G. de Boer and W.W. van den Hoogenhof
(With 4 Figures) 119

Investigation of the Heavy-Atom Distribution in a Langmuir–Blodgett Film by an X-Ray Total External Reflection and Fluorescence Study
By S.I. Zheludeva, M.V. Kovalchuk, N.N. Novikova, I.V. Bashelhanov, T. Ishikawa, and K. Izumi (With 2 Figures) 125

A Structural Investigation of an Ultra-Thin Langmuir–Blodgett Film by an X-Ray Standing Wave Excited in a LSM Substrate Under the Bragg Diffraction Condition
By M.V. Kovalchuk, S.I. Zheludeva, N.N. Novikova, I.V. Bashelhanov, M.J. Bedzyk, and G.M. Bommarito (With 1 Figure) 129

Part IV Liquid Surfaces

The Structure of Self-Assembled Monolayers
By P. Eisenberger, P. Fenter, and K.S. Liang (With 1 Figure) 135

Behenic Acid as a Structural Model for Fatty Acid Monolayers at the Air/Water Interface: An X-Ray Diffraction Study
By R.M. Kenn, C. Böhm, H. Möhwald, K. Kjaer, and J. Als-Nielsen (With 3 Figures) 139

X-Ray Scattering Studies of Organic Monolayers on Electrolytic Solutions: Arachidic Acid on $CdCl_2$
By K. Kjaer, J. Als-Nielsen, R.M. Kenn, C. Böhm, P. Tippmann-Krayer, C.A. Helm, H. Möhwald, F. Leveiller, D. Jacquemain, M. Lahav, L. Leiserowitz, and M. Deutsch (With 3 Figures) 143

The Phases of Phosphatidyl Ethanolamine Monolayers
By C.A. Helm, P. Tippmann-Krayer, R.M. Kenn, H. Möhwald, J. Als-Nielsen, and K. Kjaer (With 2 Figures) 147

X-Ray Diffraction Studies of Fatty Acid Monolayers on the Surface of Water
By M.C. Shih, T.M. Bohanon, J.M. Mikrut, P. Zschack, and P. Dutta (With 2 Figures) 151

Protein Recognition Processes at Functionalized Lipid Surfaces: A Neutron Reflectivity Study
By D. Vaknin, J. Als-Nielsen, M. Piepenstock, and M. Lösche (With 1 Figure) 155

Neutron Reflection from Liquid/Liquid Interfaces
By T. Cosgrove, A. Eaglesham, D. Horne, J.S. Phipps, and R.M. Richardson (With 5 Figures) 159

Polymer Interfaces Analysed on a Nanometer Scale: X-Ray and Neutron Reflectometry
By M. Stamm 167

Neutron Reflection from Polymers Adsorbed at the Solid/Liquid Interface
By T. Cosgrove, J.S. Phipps, and R.M. Richardson
(With 3 Figures) 169

Part V Electrochemistry

Electrochemical Roughening of Au(110) Single Crystal Electrodes
By K.M. Robinson, W.E. O'Grady, and I.K. Robinson
(With 1 Figure) 175

Part VI Thin Films and Multilayers

Reflectivity Studies of Thin Au Films and Au Bicrystals with Grain Boundaries
By E. Burkel, M. Fitzsimmons, and M. Müller-Stach
(With 3 Figures) 181

Depth Resolved Diffuse Scattering from Buried $CoSi_2$ Layers in Silicon
By D. Bahr, B. Burandt, M. Tolan, W. Press, R. Jebasinski, and S. Mantl (With 2 Figures) 187

Glancing Angle X-Ray Techniques for the Analysis of Ion Beam Modified Surfaces
By T.A. Crabb and P.N. Gibson (With 3 Figures) 191

Surface Analysis of Borkron Glass for Neutron Applications
By M. Maaza, C. Sella, B. Farnoux, F. Samuel, and P. Trocellier
(With 3 Figures) 195

X-Ray Bragg Reflectivity of ErAs Epitaxial Films
By P.F. Miceli, C.J. Palmstrøm, and K.W. Moyers
(With 4 Figures) 203

Measurement of Magnetic Field Penetration Depth in Niobium Polycrystalline Films by the Polarized Neutron Reflection Method
By L.P. Chernenko, D.A. Korneev, A.V. Petrenko, N.I. Balalykin, and A.V. Skripnik (With 1 Figure) 209

Neutron Reflectivity Studies on Superconducting, Magnetic and Absorbing Thin Films on the Polarized Neutron Spectrometer at the Pulsed Reactor IBR-2
By D.A. Korneev, V.V. Pasyuk, A.V. Petrenko, and E.B. Dokukin
(With 3 Figures) 213

Magnetic Properties of Ultrathin Co/Ag Films Investigated by Polarised Neutron Reflection
By H.J. Lauter, J.A.C. Bland, R.D. Bateson, and A.D. Johnson (With 3 Figures) 219

Depth Selective Real Structure Analysis of Semiconductor Superlattices Using Grazing Incidence X-Ray Diffraction
By U. Pietsch (With 2 Figures) 223

Investigation of Interfaces with Grazing Incidence Neutron Radiation
By V.I. Mikerov, A.V. Vinogradov, I.V. Kozhevnikov, F.A. Pudonin, V.A. Tukarev, and M.P. Yakovlev (With 5 Figures) 227

Roughness Characterization of the Surface and Interface of MBE-Grown Thin Films
By A. Stierle, A. Abromeit, K. Bröhl, N. Metoki, and H. Zabel (With 3 Figures) 233

Part VII **Instrumentation and Methods**

Neutron Diffraction Under Grazing Incidence: Recent Results from the Evanescent Wave Diffractometer
By K. Al Usta, H. Dosch, A. Lied, and J. Peisl (With 5 Figures) 239

Analytical Calculation of the Resolution Correction Function for X-Ray Surface Structure Analysis at High Exit Angles
By C. Schamper, H.L. Meyerheim, W. Moritz, and H. Schulz (With 2 Figures) 247

Neutron Double Crystal Diffractometry – A Precise Method for Surface Investigations
By F. Eichhorn, K.M. Podurets, S.Sh. Shilstein, and Z.N. Soroko (With 4 Figures) 251

Index of Contributors 255

Analytical Calculation of the Resolution Correction Function for X-Ray Surface Structure Analysis at High Exit Angles

C. Schamper, H.L. Meyerheim, W. Moritz, and H. Schulz

Institute of Crystallography and Mineralogy, University of Munich, Theresienstr. 41, W-8000 München 2, Fed. Rep. of Germany

Abstract. The analysis of rod scans in surface x-ray diffraction provides information about structure parameters normal to the sample surface. In order to achieve high resolution the measurements have to extend to momentum transfers q_z as large as possible. The proper correction of the measured intensity data for the resolution function of the detector is a prerequisite for obtaining reliable structure information. We have developed an analytical expression for the resolution correction of rod scan intensity data which take into account an anisotropic detector resolution $T(\Theta,\Phi)$, the domain size of the sample, ζ, and the primary beam divergence parallel to the sample surface $\Delta\tau$.

1. Introduction

Glancing incidence angle x-ray scattering is now a well established technique for surface structure analysis [1,2]. So far work has been concentrated on measurements of 'in plane' data providing only the projection of the structure. In order to obtain infomation about the structural parameters normal to the sample surface, measurments along the reciprocal lattice rods up to high momentum transfer $q_z=\ell\cdot c^*$ have to be performed. However, in all diffraction experiments the measured intensities have to be corrected for the instrumental resolution. For in plane structure analysis this is simply done by multiplying the intensity by a factor Δq_z corresponding to the length of the rod accepted by the detector [1,2].

The correction factors become complicated for rod scans, when the scattering plane is no longer parallel to the sample surface. In the following we shortly outline the intensity correction due to the detector resolution for our z-axis diffractometer with two independent detector angles. Subsequently we discuss the results by considering different detector arrangements, where the primary beam divergence and the finite domain size of the sample are taken into account.

2. Calculation

Experimentally, the integrated intensity is measured by rotating the sample around the surface normal keeping the detector at a fixed position out of plane. In Fig.1 this procedure is shown in projection to the $\ell=0$ plane when the reciprocal lattice rod is swept through the detector's aperture. The integrated intensity is given by the convolution of the reflectivity with the transmission function:

Springer Proceedings in Physics, Vol. 61 Surface X-Ray and Neutron Scattering
Eds.: H. Zabel and I.K. Robinson

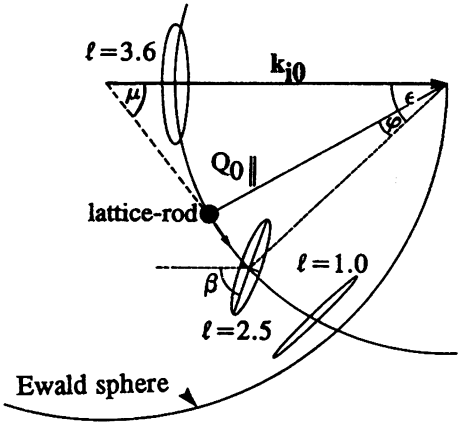

Fig. 1: Projection of the diffraction geometry on the $\ell=0$ plane, illustrating the measurement of the integrated intensity. The sample is rotated around the surface normal. Diffraction is obtained when the rod intersects the detector aperture. The angular range of φ where the rod remains within the detector changes at different ℓ values. The measured intensities must therefore be corrected due to the different shapes of the resolution ellipse.

$$E(Q_0) \propto \iiint i(k_i - k_{i0}) \cdot |F(q)|^2 \cdot$$
$$\cdot\, T(q - Q_0 - \Delta Q_1(k_i - k_{i0}) - \Delta Q_2(\varphi))\, dq^3\, dk_i^3\, d\varphi \quad . \tag{1}$$

In Eq. 1 $i(k_i - k_{i0})$ describes the intensity distribution in the primary beam around the incident beam k_{i0}. Gaussian functions are assumed for the primary beam intensity distribution i, the transmission function T and the rod profile parallel to the surface $|F(q_\parallel)|^2$. The parameters q and Q_0 represent vectors in reciprocal space, the latter indicates the reflection under consideration. The primary beam divergence and the rotation angle φ of the crystal are taken into account by the arguments $\Delta Q_1(k_i - k_{i0})$ and $\Delta Q_2(\varphi)$. The calulation is based on three assumptions: (1) a grazing incidence geometry is used, (2) the radiation is strictly monochromatic and (3) the lateral extensions of the reciprocal lattice rod and the detector acceptance are small as compared to the radius of the Ewald sphere. The analytic solution of Eq. (1) is simple but tedious and will be described elsewhere [3]. Finally we are left with an expression $E(Q_0) \propto |F(Q_0)|^2 \cdot L(Q_0)$, where

$$L(Q_0) = \frac{\lambda \cdot \Delta\Theta \cdot \Delta\Phi}{d^{1/2} \cdot a \cdot b \cdot |Q_{0\parallel}|} \left\{ 1 + m \cdot \Delta\tau^2 \cdot \Gamma^2 + m/\zeta^2 \right\}^{-1/2} \tag{2}$$

indicates the Lorentz factor which describes the dependence of the integrated intensity on pure geometric parameters, particularly on the acceptance angles of the detector $\Delta\Theta$ and $\Delta\Phi$. The parameters d, m and Γ are given by

$$c = \cos(\beta-\epsilon) \cdot \cos(\beta-\epsilon) \cdot (1/a^2 - 1/b^2) \tag{3}$$
$$d = (\sin(\beta-\epsilon))^2 / a^2 + (\cos(\beta-\epsilon))^2 / b^2 \tag{4}$$
$$e = (\cos(\beta-\epsilon))^2 / a^2 + (\sin(\beta-\epsilon))^2 / b^2 \tag{5}$$

$$m = \lambda^2 \cdot (e - c^2/d) \qquad [\text{Å}^2] \qquad (6)$$

$$\Gamma = (\cos \mu) / \lambda - | Q_{0l} | \cdot \cos (\mu + \epsilon), \qquad [\text{Å}^{-1}] \qquad (7)$$

where a/λ and b/λ [Å^{-1}] are the short and the long axis of the projected resolution ellipse, respectively (Fig. 1) and μ is the projection of the scattering angle to the surface. The angles β and ϵ are explained in Fig. 1. The Lorentz factor factor given by Eq. (2) is composed of two terms, the first representing the intensity correction assuming δ-function like lattice rods and strictly parallel incident radiation, the second (under the square root) takes account for the domain size, ζ, and the primary beam divergence $\Delta\tau$. In the low exit angle regime ($\ell \leq 1$) the correction calculated from Eq. (1) agrees with the published formula [1,2], provided that the domain size ζ is large and the primary beam is parallel ($\Delta\tau=0$).

3. Results and Discussion

In order to elucidate the different factors contributing to the intensity corrections we have calculated $L(\ell)$ for the (1/2 1/2) and (3/2 5/2) superlattice reflection rod of the Ge(001)(2x1) structure assuming a wavelength of $\lambda = 1.54$ Å. The results are shown in Fig. 2. In order to maximize the intensity at low ℓ it is evident that the detector has to be aligned with a high acceptance parallel to the rods. However, the situation changes at intermediate and high ℓ, where the intersection of the lattice rod with the Ewald sphere crosses the detector transmission increasingly oblique to the long axis. Under these conditions it is preferable to rotate the detector by 90°, as displayed in Fig.1. Additionally, the dependence on Q_{0l} results in an about four times larger intensity of the (1/2 1/2 ℓ) as compared with the (3/2 5/2 ℓ) reflections for $\ell \leq 1$.

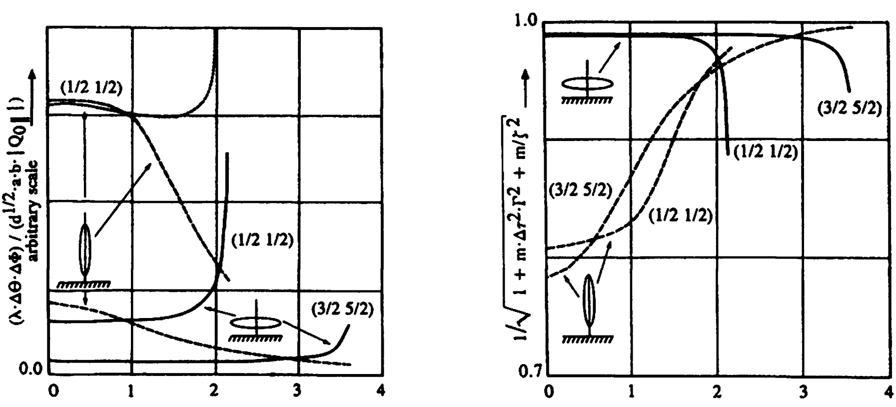

Fig. 2: Lorentz factor as a function of ℓ for both detector settings (solid and dashed line) assuming parallel primary beam and δ-like rods (left panel). The detector acceptance angles are 0.4° and 2.0°. The dotted line indicates the resolution correction for the (1/2 1/2) rod as given by ref. [2]. The right panel shows the ℓ-dependence of the correction term in Eq. 2 for a domain size ζ of 500 Å and a beam divergence $\Delta\tau$ of 0.23°.